

Using Automatic HARDI Feature Selection, Registration, and Atlas Building to Characterize the Neuroanatomy of $A\beta$ Pathology

Evan Schwab¹, Michael A. Yassa², Michael Weiner³, René Vidal¹

¹Center for Imaging Science, Johns Hopkins University

²Department of Neurobiology and Behavior, University of California, Irvine

³Department of Radiology, University of California, San Francisco

Abstract. The detection of white matter microstructural changes using diffusion magnetic resonance imaging (dMRI) often involves extracting a small set of scalar features, such as fractional anisotropy (FA) and mean diffusivity (MD) in diffusion tensor imaging (DTI). With the advent of more advanced dMRI techniques, such as high angular resolution diffusion imaging (HARDI), a number of mathematically inspired new scalar features have been proposed. However, it is unclear how to select the most biologically informative combinations of features for biomarker discovery. This paper proposes an automatic HARDI feature selection algorithm which is based on registering HARDI features to feature atlases for optimal clinical usability in population studies. We apply our framework to the characterization of beta-amyloid ($A\beta$) pathology for the early detection of Alzheimer’s disease (AD) to better understand the relationship between $A\beta$ pathology and degenerative changes in neuroanatomy.

1 Introduction

Over five million Americans suffer from Alzheimer’s disease (AD) today. Since the damage to the brain caused by AD is irreversible and the first symptoms appear when the disease is already sufficiently advanced, it is very important to establish indicators of AD (i.e., biomarkers) during the preclinical stage that allow for early diagnosis and intervention. Beta-amyloid ($A\beta$) pathology is thought to play an important role in AD pathophysiology, but the relationship between $A\beta$ pathology and structural changes in brain connectivity during the preclinical stage is not well understood. Currently, our understanding of changes in the white matter (WM) of the brain that occur early in the course of the disease is largely based on studies that use diffusion tensor imaging (DTI) to find changes in fractional anisotropy (FA) and mean diffusivity (MD) [6, 19, 20]. A major concern for DTI is its inability to resolve subvoxel crossing, bending, and twisting fibers due to limitations inherent in the single-direction tensor model and these limitations are observed in the ambiguity of FA and MD changes. This precludes accurate measurement of the complex subvoxel anatomical fiber interactions, which is important to understanding WM pathology implicated in AD.

High angular resolution diffusion imaging (HARDI) addresses the disadvantages of DTI by allowing one to estimate a multi-modal orientation distribution function from a large number of gradient directions. On the one hand, this permits defining new features with the hope of better characterizing WM structures and WM pathology. Indeed, in recent years there has been an influx of methods that generate rotation invariant HARDI features [11, 13, 14, 21, 18, 4, 15]. On the other hand, however, with so many different types of features to choose from, it is not clear which ones are most representative of neuroanatomical microstructure and most important for disease classification. Also, since many of these features are derived based on their mathematical properties, it is unclear which features are biologically relevant.

A common approach to feature selection is to use all features to train a classifier and let the classifier weights decide which features are most discriminative. This approach is appropriate for brain classification whenever the spatial location of the brain features is inconsequential. In practice, however, disease is localized in certain anatomical structures, such as the hippocampus for AD, and it is extremely important that these features be registered to a common coordinate system, or atlas, before the classifier is trained. However, the construction of the atlas and the registration algorithm are also based on the same features, and selecting which features are most relevant for registration is also an important problem. Indeed, errors in registration could incorrectly map the features to the atlas and result in incorrect classification.

Paper Contributions. In this paper, rather than addressing the feature selection problem only at the very end of the classification pipeline, we propose to automatically select anatomically informative features while simultaneously registering them and constructing a feature atlas for proper comparison of different populations. Given a collection of HARDI features extracted from multiple brain images of healthy individuals, we use them to build a HARDI atlas. This atlas is built by alternating between registering all HARDI features to a current estimate of the atlas, and recomputing the atlas by “averaging” the registered HARDI features. This is done using a generalized multi-channel large deformation diffeomorphism metric mapping (mcLDDMM) framework in which each HARDI feature is given a different weight that depends on the variance of the feature. This weight, which is estimated and updated as the atlas building algorithm proceeds, is used to automatically determine the importance of the feature for registration and atlas building. In this way, our approach embeds feature selection within a HARDI registration and atlas building framework so that the selected features, which may be important for final analysis and classification, can be optimally transferred to the atlas for training a classifier. We apply our joint feature selection, registration and atlas building framework to identify neuroanatomical differences between A β positive (+) and A β negative (–) pathologies to investigate the relationship between A β pathology and neuroanatomical degeneration in order to discover new biomarkers for AD. Our results show that the features selected automatically by our method often agree with the features that produce the most significant differences between A β + and A β –.

Paper Outline. The remainder of this paper is organized as follows: In Section 2 we review the problem of HARDI registration based on rotation invariant features. Then in Section 3 we present our joint feature selection, registration and atlas building algorithm. Finally in Section 4 we show results of our framework on a population study of $A\beta+$ and $A\beta-$ subjects to identify promising features for $A\beta$ classification.

2 Multi-Channel Registration using HARDI Features

The proposed framework for feature selection is driven by registration, whose goal is to align multiple datasets into a single coordinate system for proper comparison. Current medical image registration algorithms work very well for scalar-valued brain MRI volumes. However, for high-dimensional HARDI data, alignment requires not only warping the 3D volume of the baseline (b0) MRI, but also preserving the orientation of local diffusion information at each voxel to remain consistent within the warped neuroanatomy. To tackle this, early methods reorient the diffusion profiles after registration [1, 16]. However, this does not take into account the effect of local reorientation on the global optimization. To handle this, [8–10, 12, 24] incorporate diffusion information into the optimization. This requires computing complicated gradients and reorienting diffusivity profiles at each iteration, which can be time-consuming. Furthermore, different diffusivity profiles like the orientation distribution function (ODF), fiber orientation distribution (FOD), average ensemble propagator (EAP) or the raw signal each require a separate registration algorithm with different schemes for reorientation.

In this paper, we adopt a HARDI registration framework based on rotation invariant HARDI features. The proposed framework aligns diffusivity information accurately without having to calculate gradients or needing to reorient the data. Moreover, it can be applied to any diffusivity profile or combination thereof. More specifically, we adopt the large deformation diffeomorphic metric mapping (LDDMM) algorithm [2], which is a staple for the registration of scalar valued MRI volumes. LDDMM seeks to find an optimal diffeomorphism between two images or volumes. For registering sets of HARDI features, we use multi-channel LDDMM (mcLDDMM), which seeks to find an optimal diffeomorphism to align information contained in multiple volumes simultaneously. In particular, suppose we have C rotation invariant HARDI features for each voxel of our 3D brain volume. Let \mathcal{I}_c denote the volume of feature $c = 1, \dots, C$. Then we can represent the collection of C HARDI feature volumes by $\mathcal{I} = [\mathcal{I}_1, \mathcal{I}_2, \dots, \mathcal{I}_C]$. Now, given two collections of feature volumes $\mathcal{I}^0 = [\mathcal{I}_1^0, \mathcal{I}_2^0, \dots, \mathcal{I}_C^0]$ and $\mathcal{I}^1 = [\mathcal{I}_1^1, \mathcal{I}_2^1, \dots, \mathcal{I}_C^1]$, the goal of mcLDDMM is to find a single optimal non-linear transformation that aligns all C feature volumes jointly. That is, we wish to find a diffeomorphism φ such that $\mathcal{I}_c^1 \approx \mathcal{I}_c^0 \circ \varphi^{-1}$ for all $c = 1, \dots, C$. Since the transformation φ is the same for all c , our shorthand notation will be $\mathcal{I}^1 \approx \mathcal{I}^0 \circ \varphi^{-1}$. The diffeomorphism is generated by the flow of a family of smooth time-dependent vector fields $v_t \in \mathbf{V}$, the space of vector fields, for $t \in [0, 1]$, defined by the ordinary differential equation $\frac{d\phi_t^v}{dt} = v_t(\phi_t^v)$, where ϕ_0 is the identity transformation and $\phi_1^{v*} = \varphi^*$ is a

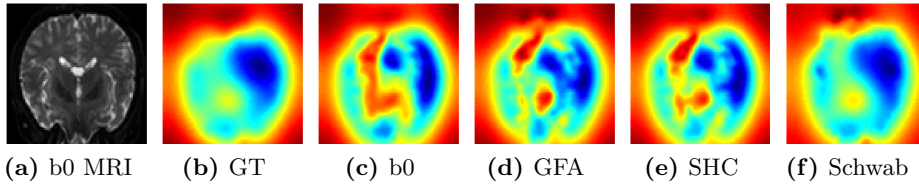


Fig. 1: Qualitative results for a semi-synthetic deformation experiment. We compare out-of-plane deformations, where blue is deformation towards the viewer and red is away from the viewer. (a) b0 MRI of the dataset. (b) ground truth (GT) deformation. (c) deformation obtained by single channel LDDMM using b0. (d) deformation obtained by DTI-like mcLDDMM using b0 and GFA. (e) deformation obtained by multi-channel LDDMM using spectral norms of spherical harmonic coefficients (SHC). (f) deformation obtained by multi-channel LDDMM using HARDI features from [21]. Note that using the features in (f) provides an estimate that is closer to the ground truth transformation.

diffeomorphic transformation defined as the solution to the following optimization problem:

$$\varphi^* = \arg \min_{\varphi} \left(\int_0^1 \|v_t(\varphi)\|_{\mathbf{V}}^2 dt + \sum_{c=1}^C \frac{1}{\sigma_c^2} \|\mathcal{I}_c^0 \circ \varphi^{-1} - \mathcal{I}_c^1\|_{L^2}^2 \right). \quad (1)$$

An optimal φ is found by gradient descent. Note that when $C = 1$, Eq. (1) reduces to the traditional single-channel LDDMM. Here the σ_c^2 are fixed weighting parameters for each channel. In most formulations, σ_c^2 is set to 1 for all c .

To illustrate the performance of mcLDDMM using various HARDI features, we generated a ground truth (GT) deformation g (Fig. 1b) by aligning a real HARDI volume A (Fig. 1a) to another real HARDI volume B (not shown) using traditional single-channel LDDMM on the b0 volumes. We then applied g to A to obtain a new transformed volume $C = A \circ g$. We compared various mcLDDMM methods with differing features to align A and C to measure which one was closest to the GT g . In Fig. 1 we show the qualitative results comparing: (Fig. 1c) LDDMM-b0, the baseline single-channel registration of b0 images, (Fig. 1d) mcLDDMM-GFA, the 2-channel registration using b0 and GFA, which is analogous to the method of [5] that uses b0 and FA for DTI, (Fig. 1e) mcLDDMM-SHC, the 5-channel registration using b0 and three SHC norms [3], (Fig. 1f) mcLDDMM-Schwab, the multi-channel registration using b0 and a set of rotation invariant features for HARDI developed in [21]. These results demonstrate that by using the features proposed in [21] we can achieve a more accurate registration than traditional LDDMM and LDDMM based on GFA or SHC. But most importantly, we wish to understand which features out of the many available in the literature are important for driving registration and which are important for disease classification. Next we present our method for automatically selecting features based on their anatomical information.

3 Automatic Feature Selection using mcLDDMM

Now that we can register HARDI features using mcLDDMM, we wish to learn which features capture the most information to drive registration and preserve the neuroanatomy. Rather than fixing each σ_c , we estimate the value of these parameters as a way of measuring their informativeness for registration. To that end, we employ an iterative algorithm that alternates between estimating the informativeness of a feature given a HARDI template (i.e., estimate σ_c) and estimating the HARDI template given the informativeness of each feature.

Our method is derived from the Bayesian template estimation work of [17], which estimates a 3D shape template for computational anatomy. The work of [7] uses the same algorithm for the single-channel HARDI registration of ODFs to build a HARDI atlas. The framework was also extended to fuse information from multiple atlases both for computational anatomy [22] and DTI [23], but the value of σ_c for each channel was kept constant. Our algorithm expands upon these prior works by using mcLDDMM to build a HARDI feature atlas while simultaneously learning the variance parameters σ_c that weight each feature channel.

More specifically, let $\mathbf{I} = \{\mathcal{I}^1, \mathcal{I}^2, \dots, \mathcal{I}^N\}$ be a collection of HARDI volumes corresponding to N normal subjects, each volume \mathcal{I}^n having C feature channels, i.e., $\mathcal{I}^n = [\mathcal{I}_1^n, \mathcal{I}_2^n, \dots, \mathcal{I}_C^n]$. Let J be a template consisting of C feature volumes $J = [J_1, J_2, \dots, J_C]$ to be estimated from \mathbf{I} . Let $\Theta = \{\theta_1, \theta_2, \dots, \theta_N\}$ be a collection of transformations from subject \mathcal{I}_n to J , such that $\mathcal{I}_n \approx J \circ \theta_n^{-1}$. Let $J^0 = [J_1^0, J_2^0, \dots, J_C^0]$ be a set of feature volumes associated to a known HARDI brain hypertemplate, and let μ be a transformation between the estimated template J and the hypertemplate, such that $J = J^0 \circ \mu^{-1}$. Under the model $p(\mathbf{I}, \Theta, \mu; \sigma) \propto p(\mathbf{I} | \Theta, \mu; \sigma)p(\Theta)p(\mu)$, the goal of atlas building is reduced to estimating a transformation μ given the observations \mathbf{I} and the hypertemplate J_0 (assuming latent variables Θ) by minimizing the negative log likelihood:

$$\begin{aligned} -\log p(\mathbf{I}, \Theta, \mu; \sigma) &= \sum_{n=1}^N \sum_{c=1}^C \frac{1}{2\sigma_c^2} \|J_c^0 \circ \mu^{-1} \circ \theta_n^{-1} - \mathcal{I}_c^n\|_2^2 + \frac{1}{2} SCN \log \sigma_c^2 \\ &+ \frac{1}{2} \|v_t(\mu)\|_{\mathbf{V}_\pi}^2 + \sum_{n=1}^N \frac{1}{2} \|v_t(\theta_n)\|_{\mathbf{V}}^2 - \log(Z_\pi) - N \log(Z), \end{aligned} \quad (2)$$

where $v_t(\mu) = \frac{d\mu_t}{dt}$ and $v_t(\theta_n) = \frac{d\theta_n}{dt}$, and Z_π and Z are normalization constants.

In theory, we could estimate σ and μ using a generalized Expectation Maximization (EM) that, at iteration k , minimizes the negative expected log likelihood:

$$\sigma_c^{2(k+1)} = \frac{1}{SCN} \sum_{n=1}^N E_{\mu^{(k)}} \{ \|J_c^0 \circ \mu^{(k)-1} \circ \theta_n^{-1} - \mathcal{I}_c^n\|_2^2 | \mathcal{I}_c^n \}, \quad (3)$$

$$\mu^{(k+1)} = \arg \min_{\mu} \left\{ \|v_t(\mu)\|_{\mathbf{V}_\pi}^2 + \sum_{n=1}^N \sum_{c=1}^C \frac{E_{\mu^{(k)}} \{ \|J_c^0 \circ \mu^{-1} \circ \theta_n^{-1} - \mathcal{I}_c^n\|_2^2 | \mathcal{I}_c^n \}}{2\sigma_c^{2(k+1)}} \right\}. \quad (4)$$

Algorithm 1 (Feature Selection and Template Estimation)

Let $J_c^{(k)}$ be the estimated template and $\sigma_c^{2(k)}$ be the estimated variances for each channel c at iteration k . For iteration $(k + 1)$,

1. Warp each subject \mathcal{I}_c^n to $J_c^{(k)}$ using mcLDDMM with parameters $\sigma_c^{2(k)}$ to obtain $\mathcal{I}_c^n \circ \theta_n^{(k)}$ with Jacobian determinant $|D\theta_n^{(k)}(y)|$ at each voxel y of the image volume.
2. Compute mean feature image

$$\bar{\mathcal{I}}_c^{(k+1)}(y) = \frac{\sum_{n=1}^N \mathcal{I}_c^n \circ \theta_n^{(k)}(y) |D\theta_n^{(k)}(y)|}{\sum_{n=1}^N |D\theta_n^{(k)}(y)|}. \quad (5)$$

3. Update noise variance feature weights by

$$\sigma_c^{2(k+1)} = \frac{1}{SCN} \sum_{n=1}^N \|\mathcal{I}_c^n \circ \theta_n^{(k)} - J_c^{(k)}\|_2^2, \quad (6)$$

where S is the total number of voxels in each volume and C is the number of channels.

4. Given $\sigma_c^{2(k+1)}$, update our template by finding the transformation that minimizes the distance between $\bar{\mathcal{I}}_c^{(k+1)}$ and J_c^0 ,

$$\mu^{(k+1)} = \arg \min_{\mu} \int_0^1 \|v_t(\mu)\|_{\mathbb{V}}^2 dt + \sum_{c=1}^C \frac{1}{\sigma_c^{2(k+1)}} \|(\bar{\mathcal{I}}_c^{(k+1)} \circ \mu^{-1} - J_c^0) \sqrt{A^{(k+1)}}\|_2^2, \quad (7)$$

and write the updated template as $J_c^{(k+1)} = J_c^0 \circ \mu^{(k+1)}$, where the weight image is given by $A^{(k+1)} = [\alpha^{(k+1)}(y)]$ for $\alpha^{(k+1)}(y) := \sum_{n=1}^N |D\theta_n^{(k)}(y)|$.

5. We repeat until $\|\sigma_c^{2(k+1)} - \sigma_c^{2(k)}\| < \epsilon$ for some small $\epsilon > 0$ for all c .

However, the expectation $E_{\mu^{(k)}} (\|J_c^0 \circ \mu^{-1} \circ \theta_n^{-1} - \mathcal{I}_c^n\|_2^2 | \mathcal{I}_c^n)$ w.r.t. Θ cannot be computed analytically due to the nonlinear dependency of this quantity in θ_n . To overcome this issue, the authors of [17] utilize the Mode Approximation Expectation Maximization (MAEM) algorithm, in which the conditional distribution of the latent variables is replaced by a Dirac measure at its mode. This leads to the MAEM Algorithm 1, where (3) and (4) are solved alternatively. To initialize MAEM, we set J^0 to be a randomly selected subject in \mathbf{I} and set $\sigma_c = 1$ for all c . Based on the findings of [17], the choice of the hypertemplate does not greatly effect the resulting template.

The MAEM algorithm results in estimated feature atlases J_c^* and weights $w_c^* = 1/\sigma_c^{2*}$ for each feature channel c . By analyzing the resulting channel weights for each of our HARDI features, we are able to automatically select the most important features that drive registration. In particular, channels with large variance σ_c^2 will receive a small weight w_c in each successive iteration. Since $w_c = 1$ is our initialization, we may identify features with $w_c^* < 1$ as less important for driving registration since they have a larger error σ_c^2 . As an extreme example, a feature that contains large amounts of noise (SNR very small) will result in large

σ_c^2 and therefore w_c^* will be small. So, HARDI features with very low SNR will be weighted lower since they do not carry consistent anatomical information. On the other hand, features with $w_c^* \geq 1$ are important for driving registration since they exhibit smaller σ_c^2 . However, features with extremely high weights may not be informative for registration. As an extreme example, a feature which is constant for every voxel in a brain volume, and therefore anatomically uninformative, will return a $\sigma_c^2 = 0$ and $w_c^* = \infty$. Thus, our template estimation algorithm can automatically select important features that drive registration by automatically adjusting the weights. These weights can be further tuned for classification by training a classifier for a specific disease application. In Section 4 we analyze the relative feature weights resulting from our algorithm with respect to A β pathology status.

4 Automatic Feature Selection, Registration, and Atlas Building Applied to Characterization of A β Pathology

In this section we will apply our automatic registration driven feature selection algorithm to characterize the WM neuroanatomy of A β pathology. Our goal is to identify features that are useful in the classification of A β pathology in order to assess novel biomarkers for the early detection of AD. To that end, we compare anatomical features selected by our algorithm with disease-specific features that present statistically significant differences in the presence of A β pathology. Our automatic feature selection will provide us with a shortlist of anatomically informative features from which a subset could be chosen that may be important for classifying A β pathology.

4.1 Extraction of HARDI Features

In recent years there have been a number of innovative frameworks for extracting new rotation invariant features from HARDI data. Here, we compare these features to understand which ones have the potential to play important roles in biomarker discovery of neurological diseases. We compare three different families of features (from Schwab et al. [21], Ghosh et al. [14] and Gur et al. [15]) extracted from three different diffusivity profiles: the raw HARDI signal, the ODF, and the FOD. From [21] we extract 30 features from the 4th order SH coefficients: 25 eigenvalues, and their variance, range, median, Frobenius-norm, and 2-norm. From [13, 14] we extract 20 features from the 4th order tensor: 12 generalized invariants ($G4$), which generate 4 basic ($S4$) and 4 principal ($J4$) invariants of homogenous polynomials. From [15] we extract 32 features of the 4th order SH coefficients: 3 coefficients contracted with coefficients (I), 11 coefficients contracted with tensors (J) and 18 tensors contracted with tensors (K). For each family of features and for each spherical function, we add the baseline MRI b0 as the first channel and GFA as the second channel for comparison.

4.2 Analysis of Selected HARDI Features Compared to $A\beta$ Pathology Status

For this study we use 15 $A\beta-$ and 17 $A\beta+$ subjects, identified with florbetapir (Amyvid) PET scans, from the Hippocampal Connectivity Project (HCP) at the Center for Imaging of Neurodegenerative Diseases (CIND) at the University of California San Francisco (UCSF). For each subject, 3 HARDI scans were acquired on a Siemens 4T scanner (128 gradient directions, 3 b0 values, FOV: 192, number of slices: 26, resolution: 1.5 mm isotropic, b-value: 1400 s/mm², TR/TE: 3500/86, 3nex averaged to enhance SNR, total protocol time: 1.35 hrs).

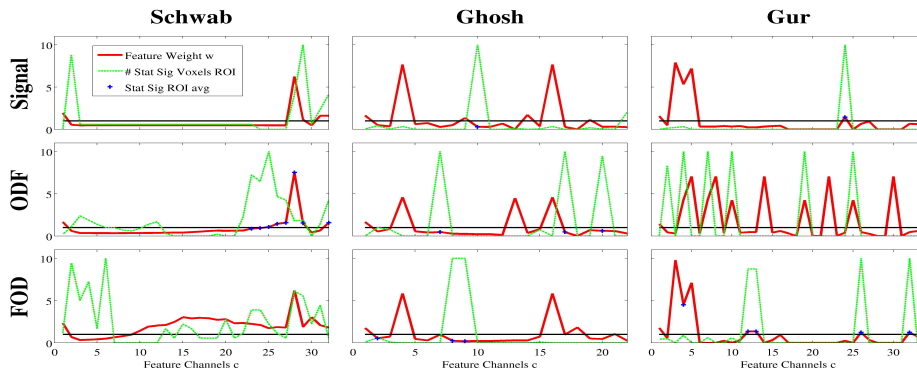


Fig. 2: Comparison of each family of features extracted from signal, ODF, and FOD after 3 iterations of Algorithm 1. Red: weights w_c for each feature channel c . Green: number of voxels in ROI that are statistically different between $A\beta+$ and $A\beta-$. Blue marker: features that have statistically significant differences in means within the ROI between $A\beta+$ and $A\beta-$. Notice that many features with high w_c (important for registration of WM) also contain statistically significant differences between $A\beta+$ and $A\beta-$.

For characterizing $A\beta$ pathology, we focus on features within the parahippocampal WM, a region of interest (ROI) that has been shown to undergo fiber degradation in aging and mild cognitive impairment [26, 25]. We first choose one subject at random among the 15 healthy subjects to be our hypertemplate J_0 . We then build feature atlases using each one of the features and HARDI functions described in Section 4.1. The resulting weights of each feature channel for each experiment after 3 iterations of Algorithm 1 are shown in red in Fig. 2. (Features whose weights were extremely high (> 20) were set to 0 in Fig. 2 only for visual comparison.) For each family, the first channel is b0 and the second channel is GFA. We also investigate feature differences between $A\beta+$ and $A\beta-$ groups after registering all subjects to the template. We ran a voxel-wise two sample paired t-test in the parahippocampal WM ROI. The number of voxels with statistically significant differences between groups is plotted in green for each feature. We also ran a two sample paired t-test on the means of the voxel values in each ROI

(left and right brain separately) and plotted features which have statistically significant mean differences as blue markers (see legend of Fig. 2).

In Fig. 3 we display a sample of feature maps for each family and function (same 3×3 grid as Fig. 2) to show the reader the types of feature maps associated to high and low weights in Fig. 2. Notice that a number of the selected features from Ghosh and Gur are not very informative, as they are either very sparse or close to a constant mask. In addition, it so happens that the methods of Ghosh and Gur produce duplicate features for different functions, as can be seen in the repeated peaks of Ghosh (channels 4 and 16 for Signal, ODF, and FOD) and Gur for ODF in Fig. 2. By looking at the results, it is evident that there is a pattern between features with weights greater than one and those with statistically significant ROI differences. However, some of the homogeneous features from Gur and Ghosh can be identified by having a peak of the number of statistically significant voxels and also have statistically significant means over the entire ROI since there is little variability. In particular, the plots of Schwab for ODF and FOD show interesting correlations and variability.

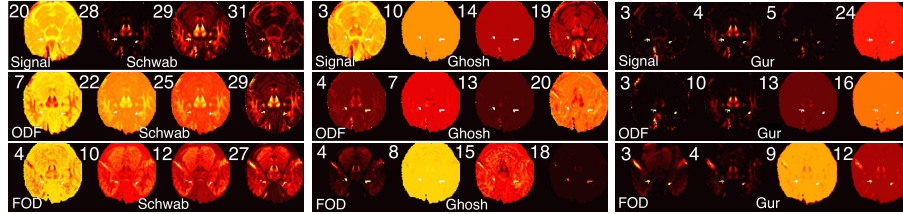


Fig. 3: Display of a subset of the feature maps obtained by each method (Schwab, Ghosh and Gur in the left, central and right columns, resp.) for each function (signals, ODF and FOD in the top, middle and bottom rows, resp.). The numbers next to each feature map correspond to the feature channel c as ordered on the x-axes in Fig. 2.

In Fig. 4 we show a subset of these statistically significant features, where the left column shows $A\beta^-$ and the right one $A\beta^+$, compared along the sagittal view of the ROI (long shaded region in black box). Common to each of these features, we notice a decrease in the intensity of each feature crossing perpendicular through the ROI. Unlike GFA, which is predominantly isotropic (blue) in the ROI, revealing little diffusivity information, some of the other selected features are able to reveal microstructural information directly crossing the parahippocampal ROI. Admittedly, when we say that a certain HARDI feature has decreased in value between $A\beta^+$ and $A\beta^-$, physical interpretations are somewhat abstract (unlike for the well defined GFA). This is definitely the case for many of the features from Ghosh and Gur which are derived mathematically. For the features from Schwab [21], it is proven that these features follow the physical distribution of the spherical function they were extracted from. Therefore, one can characterize differences in diffusivity information or physical shapes of the signal, ODF or FOD by analyzing changes in the entire set of features together instead of individual

features alone. The first row of Fig. 4 shows feature 13 of the FOD as a striking example of the differences between $A\beta+/-$. Additionally, features 10 through 27 (not shown) vary slightly from one another and all include diverse information crossing along our ROI for $A\beta+/-$.

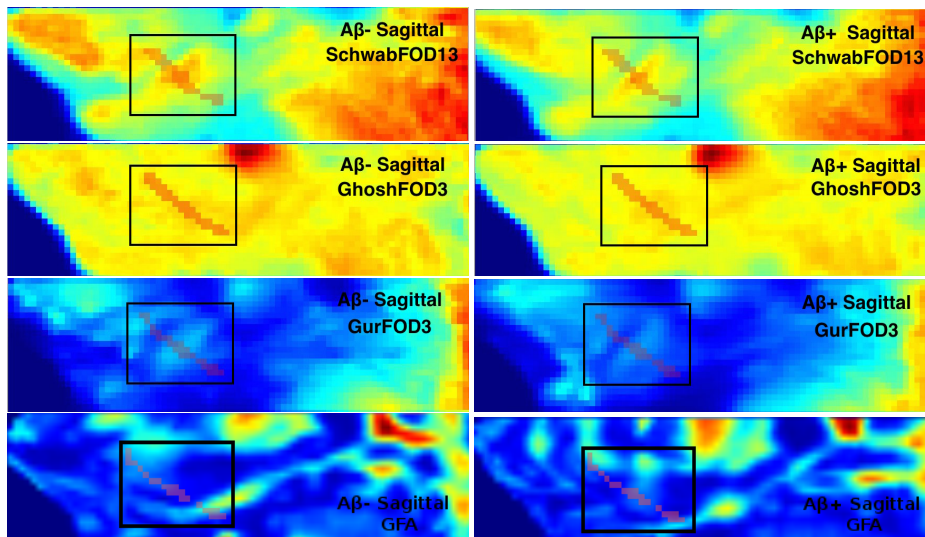


Fig. 4: Comparison of average features after registered to feature atlases. We show the sagittal view of the parahippocampal WM ROI (elongated shaded area in black box). Red: High, Blue: low. We notice a decrease in feature values crossing over ROI in Schwab, Ghosh and Gur. GFA shows little diffusivity information in ROI.

5 Conclusion

We have presented an algorithm for the joint selection, registration, and atlas building of HARDI features applied to the analysis of $A\beta$ WM pathology. This method provides an automatic way to select features that may be important for disease classification based on an anatomical criteria of registration accuracy which is not specific to a particular disease study. Then given the selected features, researchers can identify a subset based on disease classifiers. We have shown that many of the features important for registration may be useful for $A\beta+/-$ classification by showing statistically significant differences within a known ROI. We have found that the presence of $A\beta$ pathology ($A\beta+$) may be associated with feature decreases in the parahippocampal WM ROI, indicating levels of degradation in comparison to a healthy average ($A\beta-$). Our future efforts will be to incorporate these significant features into a unified classification algorithm for $A\beta$ pathology to identify potential biomarkers for the early detection of Alzheimer's Disease.

References

1. Alexander, D., Pierpaoli, C., Basser, P., Gee, J.: Spatial transformation of diffusion tensor magnetic resonance images. *IEEE Transactions on Medical Imaging* 20, 1131–1139 (2001)
2. Beg, M.F., Miller, M.I., Trounev, A., Younes, L.: Computing large deformation metric mappings via geodesic flows of diffeomorphisms. *International Journal of Computer Vision* 61(2), 139–157 (2005)
3. Bloy, L., Verma, R.: Demons registration of high angular resolution diffusion images. In: *IEEE International Symposium on Biomedical Imaging*. pp. 1013–1016 (2010)
4. Caruyer, E., Verma, R.: On facilitating the use of HARDI in population studies by creating rotation-invariant markers. *Medical Image Analysis* 20(1), 87–96 (2014)
5. Ceritoglu, C., Oishi, K., Li, X., Chou, M.C., Younes, L., Albert, M., Lyketsos, C., van Zijl, P.C.M., Miller, M.I., Mori, S.: Multi-contrast large deformation diffeomorphic metric mapping for diffusion tensor imaging. *NeuroImage* 47(2), 618–27 (2009)
6. Chao, L., Decarli, C., Kriger, S., Truran, D., Zhang, Y., Laxamana, J., Villeneuve, S., Jagust, W., Sanossian, N., Mack, W., Chui, H., Weiner, M.: Associations between white matter hyperintensities and β amyloid on integrity of projection, association, and limbic fiber tracts measured with diffusion tensor MRI. *PLoS One* 8(6), e65175 (2013)
7. Du, J., Goh, A., Qiu, A.: Bayesian atlas estimation from high angular resolution diffusion imaging (HARDI). In: *Geometric Science of Information*, pp. 149–157. Springer Verlag (2013)
8. Du, J., Goh, A., Qiu, A.: Large deformation diffeomorphic metric mapping of orientation distribution functions. In: *Information Processing in Medical Imaging*. pp. 448–462 (2011)
9. Du, J., Goh, A., Qiu, A.: Diffeomorphic metric mapping of high angular resolution diffusion imaging based on Riemannian structure of orientation distribution functions. *IEEE Transactions on Medical Imaging* 31(5), 1021–33 (2012)
10. Du, J., Hosseinbor, A.P., Chung, M.K., Bendlin, B.B.: Diffeomorphic metric mapping of hybrid diffusion imaging based on BFOR signal basis. In: *Information Processing in Medical Imaging*. pp. 1–12 (2013)
11. Fuster, A., van de Sande, J., Astola, L., Poupon, C., ter Haar Romeny, B.M.: Fourth-order tensor invariants in high angular resolution diffusion imaging. In: *Computational Diffusion MRI Workshop (CDMRI), MICCAI*. pp. 54–63 (2011)
12. Geng, X., Ross, T., Gu, H., Shin, W., Zhan, W., Chao, Y.P., Lin, C.P., Schuff, N., Yang, Y.: Diffeomorphic image registration of diffusion MRI using spherical harmonics. *IEEE Transactions on Medical Imaging* 30(3), 747–758 (2011)
13. Ghosh, A., Papadopoulos, T., Deriche, R.: Biomarkers for HARDI: 2nd & 4th order tensor invariants. In: *IEEE International Symposium on Biomedical Imaging*. pp. 26–29 (2012)
14. Ghosh, A., Papadopoulos, T., Deriche, R.: Generalized Invariants of a 4th order tensor: Building blocks for new biomarkers in dMRI. In: *Computational Diffusion MRI Workshop (CDMRI), MICCAI*. pp. 165–173 (2012)
15. Gur, Y., Johnson, C.R.: Generalized HARDI invariants by method of tensor contraction. In: *IEEE International Symposium on Biomedical Imaging*. pp. 718–721 (2014)
16. Hong, X., Arlinghaus, L., Anderson, A.: Spatial normalization of the fiber orientation distribution based on high angular resolution diffusion imaging data. *Magnetic Resonance in Medicine* 61, 1520–1527 (2009)

17. Ma, J., Miller, M.I., Trouvé, A., Younes, L.: Bayesian template estimation in computational anatomy. *NeuroImage* 42(1), 252–261 (2008)
18. Papadopoulos, T., Ghosh, A., Deriche, R.: Complete set of invariants of a 4th order tensor: The 12 tasks of HARDI from ternary quartics. In: *Medical Image Computing and Computer Assisted Intervention*. pp. 233–240. Springer (2014)
19. Racine, A., Adluru, N., Alexander, A., Christian, B., Okonkwo, O., Oh, J., Cleary, C., Birdsill, A., Hillmer, A., Murali, D., Barnhart, T., Gallagher, C., Carlsson, C., Rowley, H., Dowling, N., Asthana, S., Sager, M., Bendlin, B., Johnson, S.: Associations between white matter microstructure and amyloid burden in preclinical Alzheimer’s disease: A multimodal imaging investigation. *NeuroImage: Clinical* 4, 604–614 (2014)
20. Reijmer, Y., Fotiadis, P., Martinez-Ramirez, S., Schultz, A., Reed, A., Ayres, A., Schwab, K., Rosand, J., Viswanathan, A., Johnson, K., Greenberg, S., Gurol, E.: Microstructural white matter alterations correlate with cerebral amyloid angiopathy burden and cognitive measures: A DTI/PET study. *Neurology* 82(10) (2014)
21. Schwab, E., Cetingül, H.E., Afsari, B., Yassa, M.A., Vidal, R.: Rotation invariant features for HARDI. In: *Information Processing in Medical Imaging* (2013)
22. Tang, X., Oishi, K., Faria, A.V., Hillis, A.E., Albert, M.S., Mori, S., Miller, M.I.: Bayesian parameter estimation and segmentation in the multi-atlas random orbit model. *PLoS ONE* 8(6), e65591 (2013)
23. Tang, X., Yoshida, S., Hsu, J., Huisman, T.A., Faria, A.V., Oishi, K., Kuttner, K., Poretti, A., Li, Y., Miller, M.I.: Multi-contrast multi-atlas parcellation of diffusion tensor imaging of the human brain. *PloS one* 9(5) (2014)
24. Yap, P.T., Chen, Y., An, H., Yang, Y., Gilmore, J., Lin, W., Shen, D.: SPHERE: Spherical harmonic elastic registration of HARDI data. *NeuroImage* 55(2), 545–556 (2011)
25. Yassa, M.A., Mattfeld, A.T., Stark, S.M., Stark, C.E.L.: Age-related memory deficits linked to circuit-specific disruptions in the hippocampus. *Proceedings of the National Academy of Sciences* 108(21), 8873–8878 (2011)
26. Yassa, M.A., Muftuler, L.T., Stark, C.E.: Ultrahigh-resolution microstructural diffusion tensor imaging (msdti) elucidates perforant path degradation in aged humans in vivo. *Proceedings of the National Academy of Sciences* 107(28), 12687–12691 (2010)